SIMULATION OF SEMICONDUCTOR DEVICES AND PROCESSES Vol. 3
Edited by G. Baccarani, M. Rudan - Bologna (Italy) September 26-28, 1988 - Tecnoprint

Process Modelling and Simulator

K.Taniguchi, H.Kuroki, Y. Shibata and C. Hamaguchi
Department of Electronic Engineering, Osaka Univ.
Yamadaoka, Suita, Osaka, 565 Japan

1.Introduction

In recent and high density LSI's, optimization of scaled MOSFET demands the use of two-dimensional process and device simulators. However, process simulators now widely used have not reached a level of sophistication which allows us to predict multi-dimensional device structure and dopant profiles, especially, in submicron devices. This is due to the fact that understanding of the underlying physical and chemical processes is still insufficient to provide accurate solutions. With the present trend towards miniaturized submicrometer devices, a 2-D process models of greater sophistication has become essential to accurately optimize the fabrication process and the device structure.

In this paper, we discuss the following three topics putting special emphasis on 2-D process modeling: (1)thermal oxidation model for non-planar structure, (2)point defect based impurity diffusion model, and (3)two-dimensional ion channeling model.

2.Thermal oxidation model for non-planar structure

As the technology advances, highly nonuniform oxidation in nonplanar structures plays an important role in high packing density devices. The 2-D oxidation model proposed by Kao et al.[1-3] provides an excellent description of nonplanar oxidation in which both reaction rate and oxidant diffusivity significantly depend on stress. However, prediction of oxide structures in 2-D numerical simulation also requires accurate model of orientation dependent reaction rate at the Si/SiO_2 interface. In this work, we studied the thermal oxidation of silicon with various crystallographic orientation wafers in dry oxygen ambient. Based upon the linear-parabolic growth model[4], accurate kinetic rate constants are determined. For non-planar oxide growth simulation, a simplified reaction rate parameter is also presented.

2-1.Orientation dependence of oxidation rates

(1)Experimental procedures

All the silicon wafers used were lightly boron doped p-type silicon slices with different crystallographic orientation. The planar wafers allow full range of analytical treatment by reducing the thermal oxidation of silicon to one-dimension.

Oxidation was carried out in an ambient of dry oxygen in the 900-1100°C range for various oxidation time to obtain a variety of oxide thicknesses in the 30 - 400 nm range.

(2)Experimental results

Figure 1 shows the oxide thickness vs. oxidation time as a function of surface crystallographic orientation. Initially both the (111) and (110) orientations have the greatest rate of oxidation, the (111) becomes dominant after subsequent oxidation.

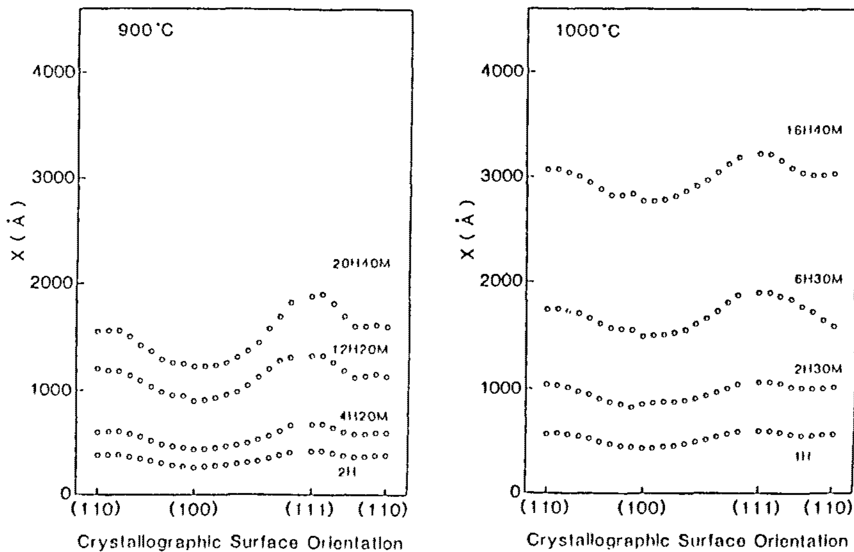

Figure 1 Oxide thickness vs. oxidation time as a function of crystallographic orientation.

(3)Parameter extraction

Using the linear-parabolic model, the oxide thickness vs. oxidation time relationship is given by

$$(X^2-X_i^2)/K_p+(X-X_i)/K_l=t \qquad (1)$$

where X is the oxide thickness, t is the oxidation time, X_i is the initial oxide thickness, and K_p and K_l are parabolic and linear rate constants. In this work, X_i is fixed to 100 A regardless of orientation and oxidation temperature because "optimum X_i" values obtained by Massoud et al.[5] are nearly constant: in the range of 85 - 117 A for the oxidation of (100)-, (111)-, (110)- oriented wafers in dry oxygen in the

900 - 1000°C range. Using the fixed X_i, a least squares fit of the data to the linear-parabolic relationship is used in the determination of the rate constants.

Figure 2 shows the linear rate constant which depends on the crystallographic orientation of the silicon substrate for all temperature range. The linear rate constant changes smoothly with substrate orientation angle.

Figure 3 shows the calculated parabolic rate constant as a function of substrate orientation. The parabolic rate constant is independent of substrate orientation above 1000°C, while at 900°C, they depend on the orientation of the underlying substrate. At 900°C, the (111) substrate orientation shows higher rate than the (100) by a factor of two.

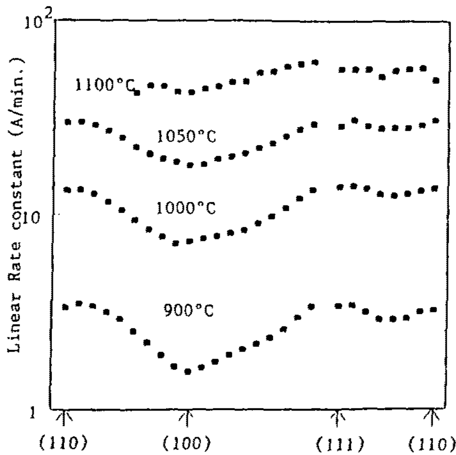

Fig.2 Linear rate constant as a function of crystallographic orientation.

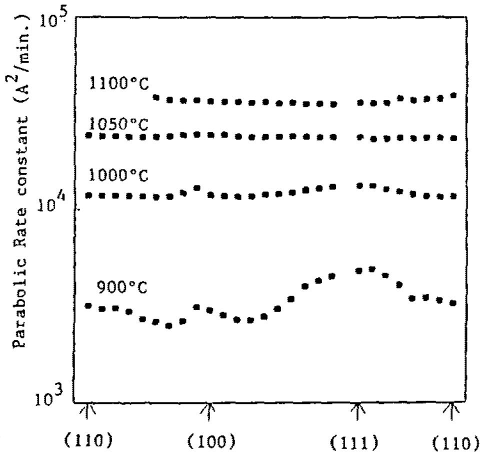

Fig.3 Parabolic rate constant as a function of orientation.

(4)Physical model of thermal oxidation

(i)Linear oxidation rate constant

Oxidation induced expansion is free in the direction towards the surface of the oxide film, but strained parallel to the surface. Unless the surface intrinsic stress is released through viscous flow of the oxide film, the generated stress make the oxidation more difficult. As pointed out by Irene,[6] oxidation rate is influenced by the film stress through which the oxide relaxes into the growth direction. However, our strain calculation reveals that the strain relaxation is not the only factor to affect the orientation dependence of oxidation rate.

The other factor to be considered is areal atomic density of silicon at the interface. In this study, we assume that areal atomic density of any plane is composed of that of three basic planes (100), (111), (110). For example, surface crystal orientation

between (100) and (111) are composed of a combination of (100) terraces and (111) ledges in ratios so as to yield the proper inclination to the (100) plane. In addition, note that the presence of the 2nd silicon layer also provides parallel oxidation sites. Therefore, the 2nd layer's contribution to the oxidation rate constant brings about "effective" areal atomic density. Hence, the orientation dependence of the reaction rate constant at the interface (linear rate constant) is well described by both strain relaxation of the oxide film and effective areal atomic density of silicon.

$$K_l = k\langle E/(1-\nu)\rangle \, \Sigma a_i N_i \qquad (2)$$

where $\langle \ \rangle$ represents the value averaged over the entire in-plane orientation[7]. E and ν are Young's modulus and Poisson's ratio, respectively. N_i is effective areal atomic density and a_i are ratios of basic planes appearing at the interface. The use of Eq.(2) in 2-D process simulator requires large computational time so that a much simpler analytical expression for K_l is preferable to simulate nonplanar oxide structure. For actual process simulation, we propose the following simplified linear rate constant

$$K_l = a_1 \sin^4(b\theta) + a_2 \sin^2(b\theta) + a_3 \qquad (0° < \theta < 54.7°)$$

$$= c_1 \cos^4(d(\theta - 54.7°)) + c_2 \cos^2(d(\theta - 54.7°)) + c_3 \qquad (54.7° < \theta < 90°) \qquad (3)$$

The parameters in Eq. (3) are tabled in Table 1.

Table 1. Parameters used in Eq.(3)

a_1=1.11	a_2=0.65	a_3=1.58 (A/min)	b=90/54.7
c_1=-.13	c_2=0.60	c_3=2.87 (A/min)	d=180/35.3

dry O_2 at 900°C

(ii)Parabolic oxidation rate constant

The parabolic rate constant K_p is independent of silicon surface orientation above 1000°C. At the high oxidation temperature, the volume change associated with the oxidation of silicon may be accommodated, at least in part, by expansion of the oxide normal to the interface because the structure of amorphous silicon dioxide is extremely flexible. Therefore, it is very likely that at high oxidation temperature, the oxide structure can relatively easily adjust itself and expand normal to the interface, thereby no change in the structure of the oxide grown on different orientations, that is, no orientation

dependence of the parabolic rate constant.

At low oxidation temperature, large film stress generated during oxidation leads to Si-O bond-breaking, especially on (111) orientation because of calculated maximum film strain on (111) plane. This structural change in turn changes the permeation rate of oxygen in the oxide, which results in high parabolic rate constant on (111) plane. The model described here is supported by the fact that the orientation dependence of the calculated film strain shows quite similar feature to that of parabolic rate constant at 900°C.

2-2.Comment on interface motion algorithm

To make simulation accurate, the physical model of oxidation process being simulated must be incorporated into the algorithms. The string algorithm widely used requires a large number of string nodes to represent non-planar $Si\text{-}SiO_2$ interface. In the two-dimensional oxidation simulators, each node representing the interface moves in a direction which is the perpendicular bisector of the normals to the two segments meeting at the node. At each time step, it is assumed that the velocities at the silicon interface is determined by using the concentration of oxidizing species at the interface[9-13]. However, the string algorithm described above is not adequate for 2-D oxidation simulator because the calculated silicon consumption is overestimated at concave structure and underestimated at convex structure. A new string algorithm which holds mass conservation should be used in a rigorous multi-dimensional process simulator.

3.Point defects based diffusion model

It is well known that the diffusion processes of dopant impurities occur via a dual mechanism[14] mediated by both the vacancy and the silicon self-interstitial. While the dual mechanism has now been firmly established, physical parameters such as diffusion coefficient of point defects, fractional interstitial component, generation and recombination rates are still uncertain. Knowing these parameters allows one to determine the 2-D distribution of the point defects by solving the diffusion equation for interstitials and vacancies. Then, dopant diffusivity at each point is coupled to the local point-defect concentration according to the equation given by[14]

$$D_A/D_A^* = f_I C_I/C_I^* + (1-f_I) C_V/C_V^* \qquad (4)$$

where D_A^* denotes the equilibrium dopant diffusivity, C_I and C_V are the interstitial and vacancy concentrations, respectively, and f_I is the fractional interstitial component.

Without knowing the parameters for point defect kinetics, no one can simulate the dopant diffusion accurately. It should be also noted that the Eq.(4) is valid only in low impurity concentration region. In high concentration region, no diffusion model based on dual mechanism is available.

3-1.Determination of point defect kinetic parameters

Simulation of 2-D dopant diffusion requires the parameters governing the kinetics of self-interstitials which play an important role in dopant diffusion process: diffusivity and surface recombination rate at the Si/SiO_2 interface. We obtained these parameters by analyzing the OSF growth at the front side and the back side of silicon wafers.

3-1-1.Diffusion constant of self-interstitials

(1)Experimental procedures

The starting substrate were p-type (100) silicon wafers with a resistivity of 6-8 ohm-cm. The wafers were implanted with boron ($1x10^{14}$ atoms/cm^2, at 80 KeV) to provide OSF nucleation sites. The wafers were oxidized at 1100°C in wet O_2 for 50 minutes to grow OSF of 10.2 µm length. Then the samples were covered with 0.4 µm polysilicon, and 0.15 um of Si_3N_4 were deposited on the polysilicon at 800°C. After removing all the films from the back side of the wafers, exposed silicon was etched off to reduce the thickness of wafers to the range of 10 to 100 µm.

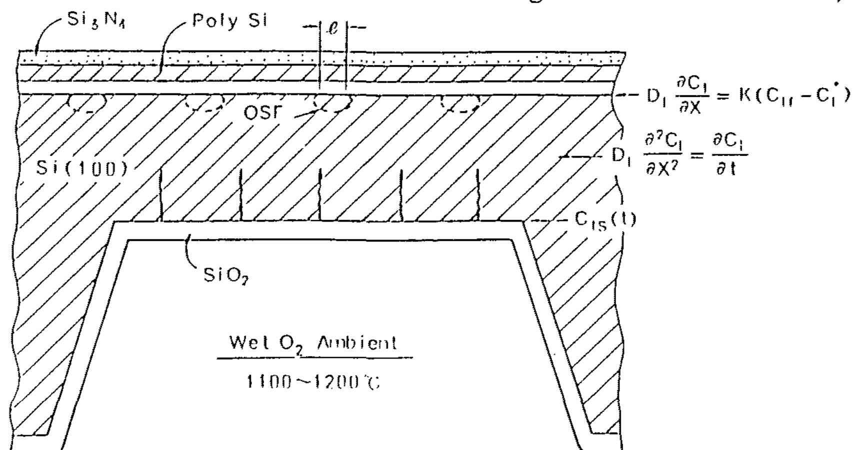

Fig.4 Sample structure used for back side oxidation

The sample structure used in this study is shown in Fig. 4. After the back side of the wafers was oxidized at various temperature in wet O_2 ambient, all films were removed and the OSF at the front surface of the samples were revealed by etching with a Wright etchant for 45 sec.

(2)Experimental results

Figure 5 shows the relationship between OSF length and oxidation time as a function of thickness of silicon. The OSF length increases with oxidation time for less than 40 μm-thick samples. The OSF length decreases and then increases with oxidation time for 80 um sample. For the 500 μm-thick sample, OSF length decreases monotonically with oxidation time and OSF vanish after 200 min.

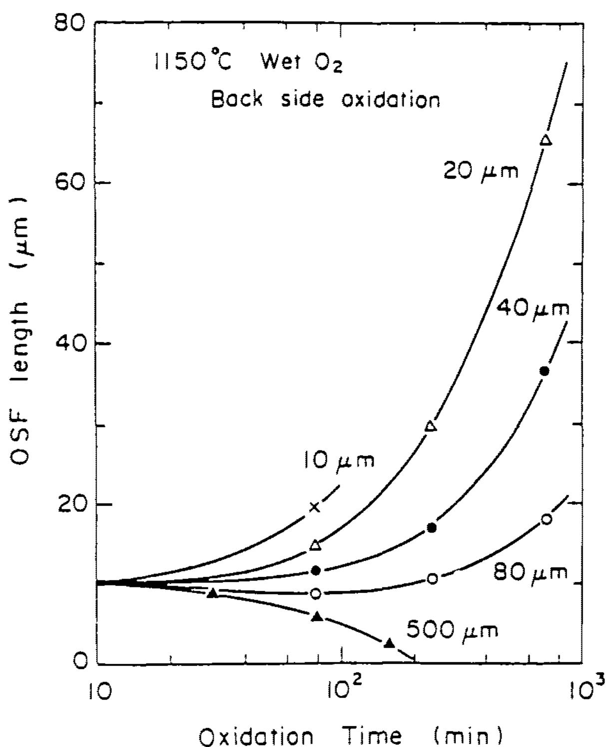

Figure 5 OSF length vs. oxidation time as a parameter of thickness of silicon.

(3)Physical model

The behavior of OSF shown in Fig. 5 can be explained by the following model. During back side oxidation, self-interstitials generated at the back Si/SiO_2 interface diffuse into bulk silicon. After a certain time, they reach the front interface and the OSF begin to grow. Until the interstitials reach the front surface, the OSF continue to shrink because the

concentration of self-interstitials at the front surface is less than that in equilibrium with the faults.

(4)Parameter extraction

In order to estimate diffusion coefficient of self-interstitials, we simulated the OSF growth by assuming that the diffusion of self-interstitials is described by a simple diffusion model with constant diffusivity in the bulk silicon. At the front surface, the flow of self-interstitials into the interface is assumed to be proportional to the excess self-interstitial concentration. The boundary conditions for self-interstitial diffusion are shown in Fig. 4. Best fit to the experimental data yields the diffusion coefficient of self-interstitials as

$$D_I = 8.6\text{x}10^5 \exp(-4.0\text{eV}/kT) \text{ cm}^2/\text{sec}. \quad (5)$$

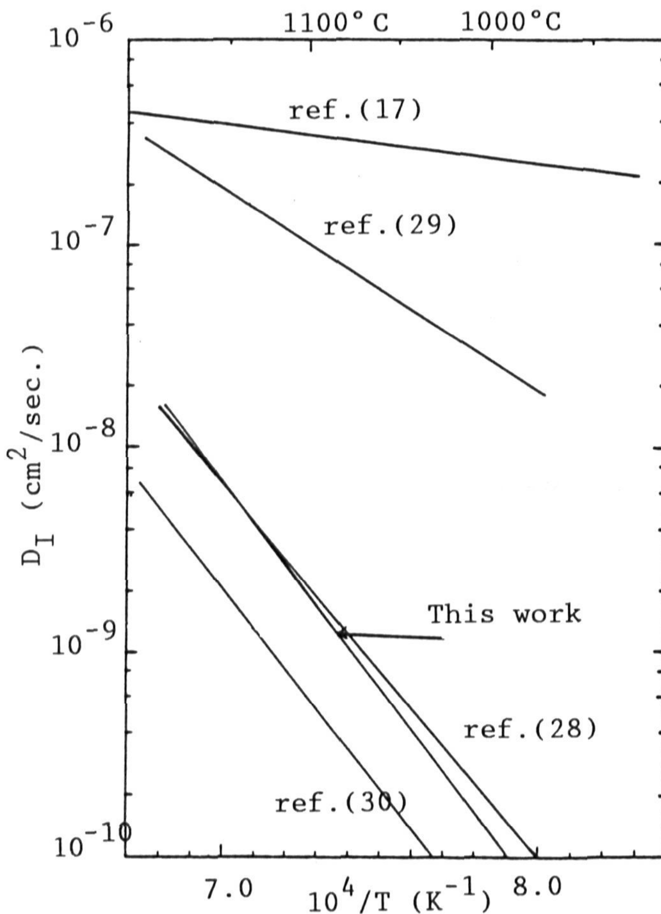

Figure 6 Diffusion coefficient of self-interstitial.

The diffusion coefficient is shown in Fig. 6 together with other published data. Although the published data scatter in a wide range, the diffusion coefficients of self-interstitials reported in recent years come to close with each other: D_I is the order of 10^{-9} cm^2/sec at 1100°C.

3-1-2.Recombination constant at the interface

(1)Experimental procedures

The starting substrate for the experiments was n-type wafers of CZ (100) silicon with a resistivity of 6-8 ohm-cm and the oxygen concentration of $0.9x10^{18}/cm^3$. The wafers were implanted with boron at a dose of $1x10^{14}/cm^2$, at an energy of 80 KeV in order to introduce controlled densities of OSF nuclei. The wafers were oxidized at 1000°C for 60 min. in dry oxygen ambient to grow OSF of 0.5 µm. Nitride film was deposited on the oxide and subsequently was photolithographically patterned into parallel stripes running across the entire wafer. Then, oxidation was carried out at temperatures in the range of 1050 - 1150°C in wet oxygen ambients. The oxide was then etched off in buffered HF, and stacking fault features were revealed by etching oxide free wafers in a Secco etch solution for 15 seconds.

(2)Experimental results

Figure 7 shows OSF's grown at the Si/SiO_2 interface near the edge of silicon nitride mask. The OSF length measured is plotted as a function of the distance from the oxidation mask edge in Fig. 8, which shows that OSF length decreases sharply with distance from the oxidation mask edge.

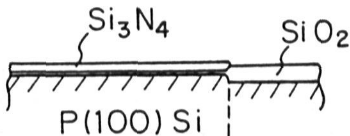

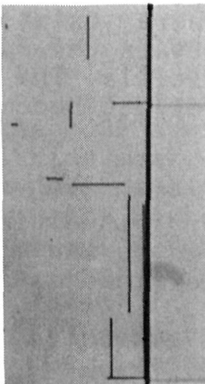

Figure 7 Photomicrograph of OSF's near the edge of silicon nitride mask.

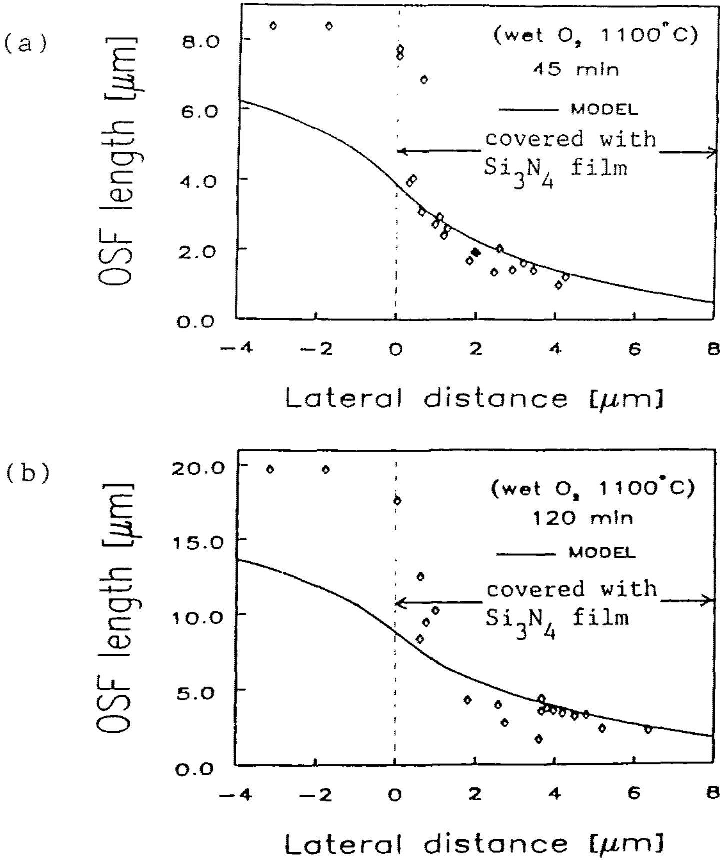

Figure 8 OSF length vs. lateral distance from nitride mask edge: (a) 45 min. and (b) 120 min. oxidation.

(3)Physical model

In order to evaluate surface recombination rate of self-interstitials, we assume that the Frank partial dislocation bounding the OSF acts as a sink or a source of self-interstitials. There exists an equilibrium concentration, C_I^{SF}, between the capture and the emission of the self-interstitials. The basic formulation of the OSF growth rate, dl/dt, becomes[15]

$$dl/dt=K(C_I-C_I^{SF}) \qquad (6)$$

where K is a proportionality factor, involving the diffusion of self-interstitials. Based on the model of Lin et al.[15], $K(C_I^{SF}-C_I^*)$ has been determined as[16]

$$K(C_I^{SF}-C_I^*)=2.3\times10^{10}\exp(-4.9\mathrm{eV}/kT)\ \mathrm{cm/sec}. \qquad (7)$$

In a structure partially covered by nitride film such as LOCOS, the silicon self-interstitials generated at the oxidizing interface are expected to flow vertically into the substrate as well as laterally into the areas adjacent to the nonoxidized region. Consequently, the self-interstitial distribution is two-dimensional nature.

By using the equations described above together with self-interstitial generation model proposed by Hu[32], we calculated the normalized excess self-interstitial concentration in the bulk as shown in Figures 9 and 10. By comparing between experimental and theoretical results, surface recombination rate was obtained. In this calculation, we assumed that the vacancy concentration is unaffected by the self-

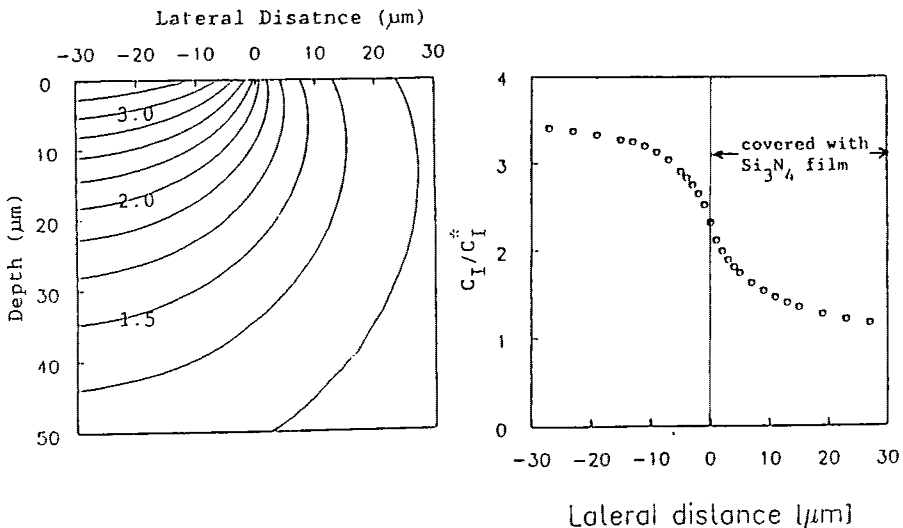

Fig.9 Excess C_I distribution near the edge of silicon nitride mask.

Fig.10. Excess C_I concentration at the Si/SiO_2 interface.

interstitials generated at the interface. The best-fitted surface recombination rate of self-interstitials is shown in Fig. 11[27-31].

(4)critical issue of flux balance model

It should be noted here that the best fit curve is in good agreement with the experimental data only for the OSF's which grow more than 1 um apart from the nitride mask edge (At each location, maximum OSF length has physical meaning[27]). Large discrepancy between the experimental and simulated results is observed in the oxidized region near the edge of the nitride mask. This indicates that the model now widely used in 2-D process simulation fails to explain the experimental results: The model predicts that the generated self-interstitials at the

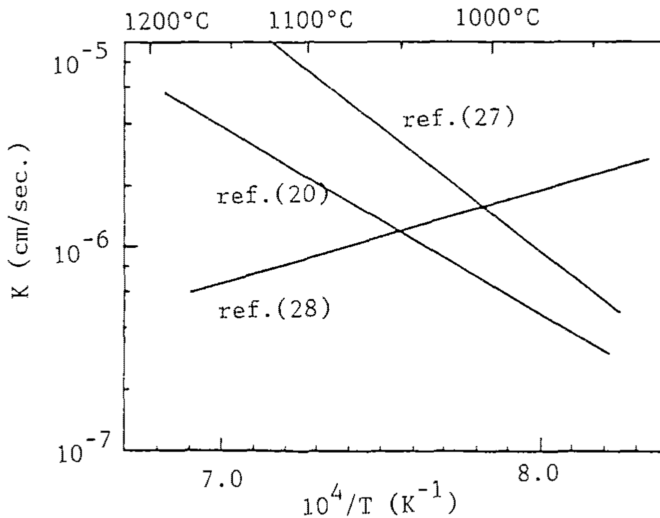

Figure 11 Surface recombination velocity as a function of temperature.

oxidizing interface adjacent to the nonoxidized region diffuse vertically as well as laterally into the bulk silicon so that the self-interstitial concentration appreciably decreases near the edge of nitride mask. The feature described above was not the case in our experiment. The experimental results suggest that the generation and recombination balance model for self-interstitial does not hold at the oxidizing interface. Therefore, self-interstitial diffusion model[32] reported so far is not suitable for the simulation of 2-D dopant diffusion especially near the edge of the nitride mask. The experimental results support the idea that the self-interstitial concentration at the oxidizing interface is uniquely determined by the oxidation rate regardless of the location of the nitride mask edge.

$$C_I/C_I^* = A(dX_{ox}/dt)^n + 1.0 \tag{8}$$

At the non-oxidized interface, the flow of self-interstitials into Si/SiO_2 interface is proportional to the concentration of self-interstitials at the interface:

$$D_I\ \mathrm{grad}(C_I) = k(C_I - C_I^*) \tag{9}$$

The two boundary conditions described above should be used for the simulation of two-dimensional dopant diffusion instead of widely accepted flux balance model[32].

3-2.Comment on dopant diffusion model parameter

Equation (4) indicates that dopant diffusivity is determined by local defect densities of both vacancies and self-interstitials. However, the reported values of fractional interstitial component, f_I, scatter in a wide range[17]. This may be attributed to the difference of estimated excess self-interstitials generated at the interface during oxidation.

Reported temperature dependence of the fractional interstitial component[18,19] is highly questionable because the fractional interstitial component predicts more than one at very high temperature, losing physical meaning. Based on a thermodynamic theory, the fractional interstitial component is expressed in the following form[20,21].

$$f_I=(1+A\ \exp(\Delta E/kT))^{-1} \qquad (7)$$

ΔE is composed of formation and migration energies for both vacancy and self-interstitial. From the experimental results of oxidation enhanced diffusion, we obtained $A=5.8\times10^{-8}$ and $\Delta E=1.77eV$ for phosphorus diffusion.

4.Two-dimensional ion channeling model

With a further refinements in integrated circuit processing, lateral diffusion distances have been significantly reduced. It is therefore becoming important to calculate accurate ion profile. Most of the ion implantation models extensively used consider the target to be amorphous in order to simplify the calculations. In practice, substrates are crystalline; there are certain axes within the crystal along which the stopping power for an ion moving is much less than for motion in a random direction, resulting in a channeling tail to the amorphous distribution. The purpose of this section is to investigate how the channeling effects affect the 2-D ion implantation profile, especially at the edge of ion implantation mask.

(1)Numerical calculation

In order to simulate 2-D ion implantation profiles, numerical technique based on Boltzmann transport equation has been developed[22,23]. The feature of this method is that energetic ion distribution is described by a function F(p,r) giving the number of ions with momentum p at location r in the target. Based on the Boltzmann transport equation, this distribution changes through the target in terms of the differential scattering cross section.

The cross section consists of an elastic and a inelastic losses. The elastic loss due to binary collisions with target atoms is calculated using the analytic form of the scattering integral proposed by Mueller[24]. The inelastic loss due to the interaction with the electrons in the target is described as a velocity-proportional drag force, leading to no change in the ion direction. In the numerical solution of the BTE, the ion distribution is described by an array of F_{ij}, representing the number of particles with energy E_i and direction $_j$ which involves the azimuthal angle. At each numerical integration of BTE, all particles in the discretized small phase space are distributed into eight adjacent discretized spaces according to their traveling angles. After each calculation step, ions with energy below some threshold E_t are considered stopped and removed from the distribution. Numerical integration of the BTE in this way proceeds until all of the ions have stopped.

Calculation procedures of channeling effects are as follows. At each integration step, the number of ions scattered into each channel is determined. These ions are removed from F and are transferred to an array G: We used two different arrays for random and channeling ions. We also take into account dechanneling effects due to thermal vibration of host atoms and displaced atoms from their sites. Number of dechanneling ions are assumed to be proportional to amorphous ratio calculated by deposited energy in each real space region.

(2)Results

It is generally accepted that channeling tail is greatly reduced for heavy ion implantation such as arsenic because of heavy damage formation along the ion path. However, experimental results[25,26] reveal that there exist channeling tails especially at low energy ion implantation. Two-dimensional ion distribution with channeling tail demand the use of BTE rather than the Monte Carlo approach because the channeling tail can be several orders of magnitude lower in concentration than the peak, leading to statistical noise for the Monte Carlo approach. Figure 12 shows calculated arsenic ion profile through a narrow slit into silicon. Two protruding equiconcentration lines are found to be aligned to the direction of <110>.

Figure 13 shows the ion distribution at a vertical mask edge which was superposed a single ion beam profile shown in Fig. 12 across the entire unmasked surface. Note that ion channeling has greatly disturbed the ion profile near the mask edge, making

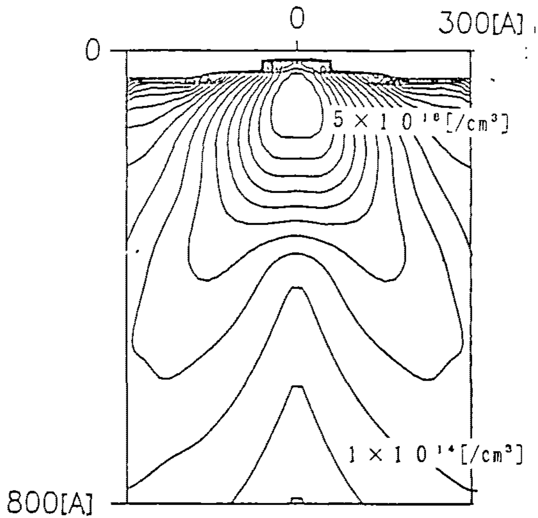

Figure 12 Calculated arsenic ion profile through a narrow slit into silicon.

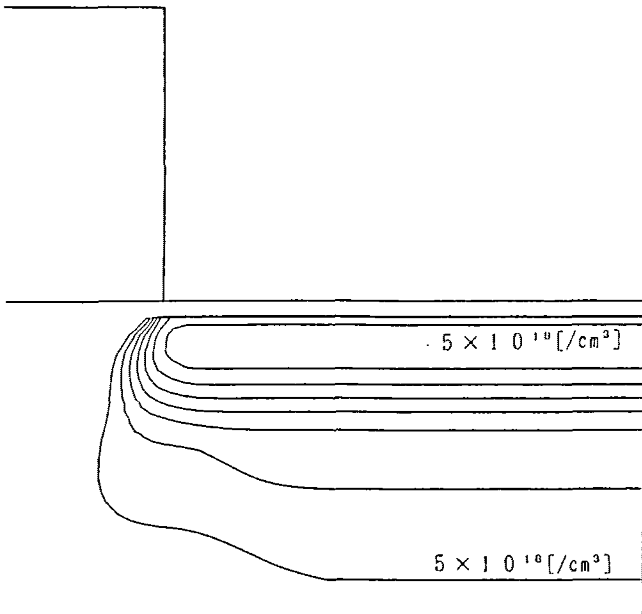

Figure 13 Arsenic ion distribution at a vertical mask edge which was superposed a single ion beam profile shown in Fig. 12 across the unmasked surface.

the calculation in amorphous target almost useless for the dopant distribution in crystalline target. Although there is no way to verify the calculated results because of the difficulty of direct measurement of two-dimensional concentration profiles, we believe that the results described above accurately reveal real ion distribution.

Acknowledgment

The authors thank Mr. K. Kobayashi of Mitsubishi Electric Corporation for the experiment of thermal oxidation of Si. One of the authors (Dr. K. Taniguchi) would like to thank Dr. D. A. Antoniadis of MIT and Dr. D. Collard of ISEN for valuable discussion on impurity diffusion.

References

1)D.B.Kao, J.P.McVittie, W.D.Nix and K.C.Saraswat, IEEE Trans. Electron Devices, ED-34, 1008 (1987)
2)D.B.Kao, J.P.McVittie, W.D.Nix and K.C.Saraswat, IEEE Trans. Electron Devices, ED-35, 25 (1988)
3)P.Sutardja, W.G.Oldham and D.B.Kao, Tech. Digest of IEDM, p.264, 1987
4)B.E.Deal and A.S.Grove, J. Appl. Phys., 36, 3770 (1965)
5)H.Z.Massoud, J.D.Plummer and E.A.Irene, J. Electrochem. Soc., 132, 1745 (1985)
6)E.A.Irene, Phil. Mag. B, 55, 131 (1987)
7)W.A.Brantley, J. Appl. Phys., 44, 534 (1973)
8)A.R.Neureuther, C.Y.Liu and C.H.Ting, J. Vac. Sci. Technol., 16, 1767 (1979)
9)D.Chin, S.Y.Oh, S.M.Hu and R.W.Dutton, IEEE Trans. Electron Devices, ED-30, 993 (1983)
10)A.Poncet, IEEE Trans. Comp. Aided Design, CAD-4, 41 (1985)
11)H.Matsumoto and M.Fukuma, IEEE Trans. Electron Devices, ED-32, 132 (1985)
12)T.L.Tung and D.A.Antoniadis, IEEE Trans. Electron Devices, ED-32, 398 (1985)
13)S.Isomae, S.Yamamoto, S.Aoki and A.Yajima, IEEE Electron Device Letters, EDL-7, 368 (1986)
14)D.A.Antoniadis, J. Electrochem. Soc., 129, 1093 (1982)
15)A.M.Lin, R.W.Dutton, D.A.Antoniadis and W.A.Tiller, J. Electrochem. Soc., 128, 1121 (1981)
16)Y.Sugita, H.Shimizu, A.Yoshikawa and T.Aoshima, J. Vac. Sci. Technol., 14, 44 (1977)
17)U.Gosele and T.Y.Tan, Proc. Material Research Soc., Vol.36, p.105, 1984
18)D.Mathiot and J.C.Pfister, Proc. Material Research Soc., Vol.36, p.117, 1984
19)S.Matsumoto, Y.Ishikawa and T.Nishi, J. Appl. Phys.

54, 5049 (1983)
20)D.Collard and K.Taniguchi, IEEE Trans. Electron Devices, ED-33, 1454 (1986)
21)P.M.Fahey, PhD Thesis, Stanford Univ., June, 1985
22)L.A.Christel, J.F.Gibbons and S.Mylroie, J. Appl. Phys., 51, 6176 (1980)
23)M.D.Giles, IEEE Trans. Computer Aided Design, CAD-5, 679 (1986)
24)G.P.Mueller, Rad. Effects Lett., 50, 87 (1980)
25)R.B.Fair, J.J.Wortman and J.Liu, J. Electrochem. Soc., 131, 2387 (1984)
26)M.Delfino, J. Electrochem. Soc., 133, 1900 (1986)
27)K.Taniguchi and D.A.Antoniadis, Appl. Phys. Lett., 42, 961 (1983)
28)P.B.Griffin and J.D.Plummmer, Tech. Digest of IEDM, p.522, 1986
29)A.Seeger and U.Gosele, Phys. Lett. A, 61, 423 (1977)
30)K.Wada and Inoue, Inst. Phys. Conf. Ser., 59, 461 (1980)
31)E.Scheid and P.Chenevier, Phys. Stat. Sol. (a), 93 523 (1986)
32)S.M.Hu, Appl. Phys. Lett., 43, 449 (1983)